Applied Physics Letters

On the focusing enhancement of Soret zone plates with ultrasound directional transducers

Cite as: Appl. Phys. Lett. **114**, 224101 (2019); https://doi.org/10.1063/1.5100219
Submitted: 16 April 2019 . Accepted: 20 May 2019 . Published Online: 06 June 2019

Sergio Pérez-López, José Miguel Fuster, Pilar Candelas, and Constanza Rubio

Applied Physics Letters ARTICLE scitation.org/journal/apl

On the focusing enhancement of Soret zone plates with ultrasound directional transducers

Cite as: Appl. Phys. Lett. **114**, 224101 (2019); doi: 10.1063/1.5100219
Submitted: 16 April 2019 · Accepted: 20 May 2019 ·
Published Online: 6 June 2019

View Online Export Citation CrossMark

Sergio Pérez-López,[1] José Miguel Fuster,[2,a)] Pilar Candelas,[1] and Constanza Rubio[1]

AFFILIATIONS

[1]Centro de Tecnologías Físicas, Universitat Politècnica de València, València 46022, Spain
[2]D. Comunicaciones, Universitat Politècnica de València, València 46022, Spain

[a)]Electronic mail: jfuster@dcom.upv.es

ABSTRACT

This work analyzes the influence of the distribution of transparent Fresnel regions over the focusing profile of Soret Zone Plates. It is shown that this effect becomes very significant in those fields where directional transducers are employed, such as microwaves or acoustics. A thorough analysis on both the lens transmission efficiency and the focusing enhancement factor is presented. Moreover, experimental measurements are also carried out, validating the theoretical model and demonstrating that the distribution of transparent Fresnel regions becomes a critical parameter in applications requiring directional emitters.

Focusing is a hot research topic in many areas of physics due to its multiple applications. Different types of lenses have been developed in order to improve the focusing performance, which includes both achieving a narrower focal area with a higher energy focus and increasing the energy efficiency of the lens. In acoustics, lenses based on planar metasurfaces have been recently presented as an alternative to traditional curved lenses. This approach employs deep-subwavelength slits[1] or coiling-up space structures[2–5] in order to generate the pressure amplitude and the phase distribution at the lens. However, these devices are usually more complex to design and manufacture than conventional lenses. In this sense, Fresnel Zone Plates (FZPs), which have been widely used in optics[6,7] and microwaves,[8,9] are simpler yet effective alternatives to conventional and metasurface-based lenses. In acoustics, FZPs have also been proposed for both air[10] and underwater[11] ultrasound focusing applications. In optics, the distance between the transducer and the lens is usually enough to consider plane wave incidence. However, in many ultrasound and microwave applications, a directional emitter is placed at a distance where the plane wave approximation is not valid. Therefore, in order to properly characterize the transmission efficiency of an acoustic lens, the influence of the transducer on the energy distribution on the lens has to be considered.

If a plane wave propagates along the z axis, the incident pressure at the lens can be described as $p_i(r) = p_0 e^{-jkz}$, where p_0 is a constant amplitude and k is the wavenumber. The incident energy (E_i) and the transmitted energy (E_t) through the lens are given by

$$E_i = \frac{1}{2\rho_0 c_0}\int\int_{S_l} |p_i(r)|^2 dS = \frac{p_0^2 \pi r_N^2}{2\rho_0 c_0}, \tag{1}$$

$$E_t = \frac{p_0^2}{2\rho_0 c_0}\int\int_{S_l} q(r) dS = \frac{\pi p_0^2}{\rho_0 c_0}\int_0^{r_N} q(r) r dr, \tag{2}$$

where ρ_0 is the medium density, c_0 is the sound velocity in the medium, r_N is the outer radius of the lens, and $q(r)$ is the pupil function of the lens. This pupil function describes the geometry of the lens, indicating whether a specific region is transparent or opaque to the ultrasound emission.

The transmission efficiency parameter, η_T, is defined as the relation between the transmitted energy through the lens transparent zones and the total incident energy at the lens. Thus, combining Eqs. (1) and (2), the transmission efficiency under plane wave incidence is

$$\eta_T = \frac{E_t}{E_i} = \frac{2}{r_N^2}\int_0^{r_N} q(r) r dr. \tag{3}$$

In the case of Soret FZPs, the pupil function is implemented using the radii of the different Fresnel regions, which can be obtained from

$$r_n = \sqrt{n\lambda F + \left(\frac{n\lambda}{2}\right)^2}, \tag{4}$$

where F is the focal distance, λ is the wavelength, and $n = 1,2, \ldots, N$, with N being the total number of Fresnel regions.

For Soret FZPs, the pupil function is 1 in the transparent regions and 0 in the pressure opaque regions. These kinds of FZPs are formed by alternating transparent and opaque regions. Thus, in the design stage, there is a degree of freedom as the central Fresnel region can be implemented with either a transparent or an opaque area. Depending on this initial choice, the remaining Fresnel regions will be implemented accordingly in an alternating distribution, as mentioned previously. Therefore, in a Soret FZP with an opaque central area (O-FZP), the transparent regions correspond to even positions ($n = 2, 4, 6, \ldots$) and $N = 2N_t + 1$, with N_t being the number of transparent regions. Alternatively, if the Soret FZP is implemented with a transparent central area (T-FZP), the transparent regions correspond to odd positions ($n = 1, 3, 5, \ldots$) and $N = 2N_t$.

In the O-FZP case, substituting Eq. (4) into Eq. (3) yields

$$\eta_T^o = \frac{1}{2}\left(1 - \frac{1 + \frac{N\lambda}{4F}}{N + \frac{N^2\lambda}{4F}}\right). \tag{5}$$

If the central region is transparent (T-FZP), the transmission efficiency can be calculated similarly as

$$\eta_T^t = \frac{1}{2} \cdot \frac{1 + \frac{\lambda}{4F}(N-1)}{1 + \frac{\lambda}{4F}N}. \tag{6}$$

As it can be deduced from Eqs. (5) and (6), if $F \gg \lambda$, transmission efficiencies can be approximated by $\eta_T^o \cong \frac{1}{2}\frac{N-1}{N}$ and $\eta_T^t \cong \frac{1}{2}$, respectively. Thus, in the O-FZP case, η_T^o tends to 50% as N increases, whereas in the T-FZP case, η_T^t tends to 50% for any value of N.

However, in real underwater ultrasound applications, a directional emitter, such as a piston transducer, is employed in most cases. These emitters present a directivity pattern with a main lobe and several secondary lobes.[12] Thus, the contributions of the different Fresnel zones across the surface of the FZP are in this case weighted by the directivity pattern of the transducer, and the inner areas contribute more significantly to the focus than the outer areas. Therefore, the design decision regarding whether the central Fresnel area is transparent or opaque becomes a critical parameter and completely changes the value of the transmission efficiency. As it can be observed from Fig. 1(a), in the O-FZP lens, the central region is opaque and blocks the main incident pressure contributions, while in the T-FZP case shown in Fig. 1(b), the central region is transparent, which allows a higher energy transmission.

In the far field, a piston transducer placed at a distance d from the lens can be modeled as a point source emitter with a given directivity pattern. In this case, the incident pressure at the lens can be expressed as

$$p_i(r) = \frac{jkp_0a^2}{2\sqrt{r^2+d^2}} D(r) e^{-jk\sqrt{r^2+d^2}}, \tag{7}$$

where p_0 is the pressure at the piston surface, a is the piston active radius, and $D(r)$ is the piston directivity pattern, which is given by

$$D(r) = \frac{2J_1(ka\sin\theta)}{ka\sin\theta}, \tag{8}$$

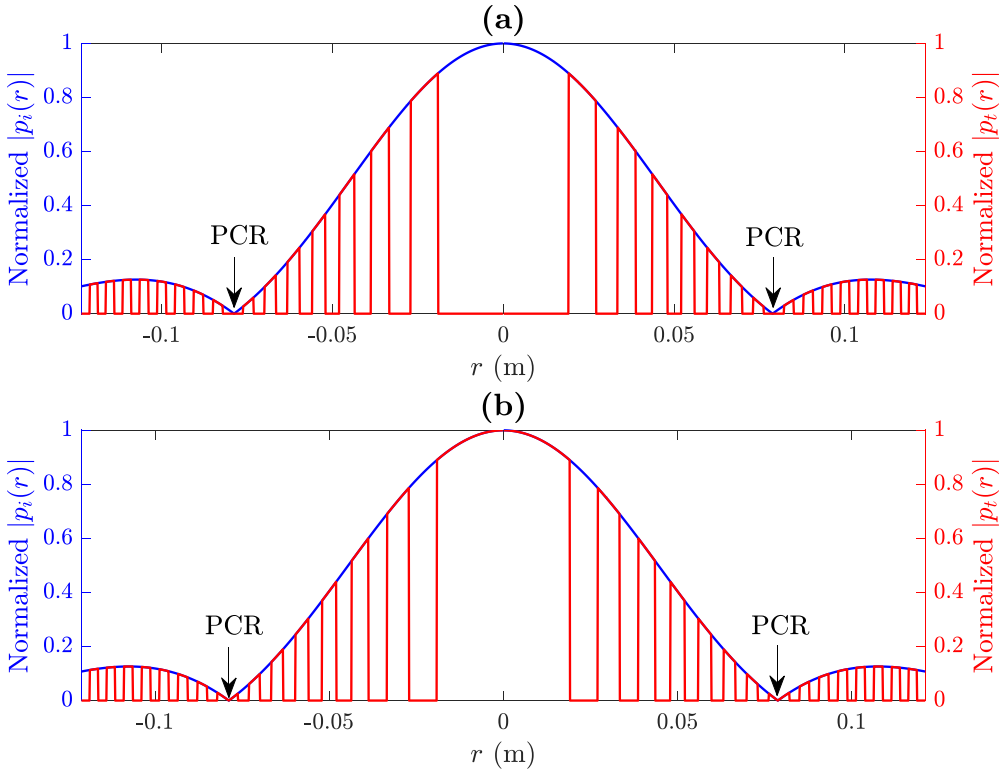

FIG. 1. Incident (blue line) and transmitted (red line) acoustic pressures in (a) O-FZP and (b) T-FZP.

with J_1 being the first kind and first order Bessel function and θ the angle referred to the normal direction of the piston surface. In this case, the different FZP radii can be calculated considering spherical wave incidence, which results in the following design expression:

$$d + F + \frac{n\lambda}{2} = \sqrt{r_n^2 + d^2} + \sqrt{r_n^2 + F^2}. \tag{9}$$

Thus, when directional transducers are considered, the lens transmission efficiency can be expressed as

$$\eta_T = \frac{\int_0^{r_N} q(r)\frac{1}{r}J_1\left(ka\frac{r}{\sqrt{r^2+d^2}}\right)^2 dr}{\int_0^{r_N}\frac{1}{r}J_1\left(ka\frac{r}{\sqrt{r^2+d^2}}\right)^2 dr}. \tag{10}$$

Figures 2(a) and 2(b) show the transmission efficiency parameter as a function of N for plane wave incidence and directional transducer, respectively. As it can be observed from Fig. 2(a), the transmission efficiency is always higher when the T-FZP lens is considered for plane wave incidence, although both T-FZP and O-FZP cases converge to approximately the same value ($\eta_T \cong 0.5$) as N increases. The slight difference in transmission efficiency is due to the fact that for the same number of transparent regions, the O-FZP implements one additional opaque region compared to the T-FZP case, which reduces the transmission efficiency. In contrast, Fig. 2(b) depicts the numerically computed transmission efficiency values for different ka factors. The ka factor provides information about the transducer size in terms of the wavelength, which means that when the ka parameter is increased, the transducer becomes more directional. As it can be seen from Fig. 2(b), in the directional emitter case, the transmission efficiency of the T-FZP is not only higher than that corresponding to the O-FZP but also significantly higher than the transmission value achieved with any FZP in the ideal plane wave case. Moreover, as ka increases, the transmission efficiency of the T-FZP augments, whereas the transmission efficiency of the O-FZP decreases. This phenomenon is a consequence of the directional behavior of the transducer, which becomes more significant for higher ka values. When the ka parameter becomes larger, a higher fraction of the incident energy is concentrated in the inner regions of the lens, and therefore, the selection of a transparent instead of an opaque central region becomes more critical.

The intensity level which can be achieved at the focus is another interesting parameter that should be considered and that characterizes the lens in terms of its focusing capabilities. A focusing enhancement factor (E_F) can be defined as $E_F = I_F^t/I_F^o$, where I_F^t represents the acoustic intensity achieved at the focus when using a T-FZP and I_F^o corresponds to that same focal intensity when focusing through the O-FZP. Figure 3 shows the enhancement factor as a function of the number of transparent Fresnel regions (N_t). The blue line represents the plane wave case, whereas red, black, and brown lines correspond to directional transducers with $ka = 10$, $ka = 15$, and $ka = 20$, respectively. As it can be observed, the enhancement factor is very close to 1 for any N_t value when plane wave incidence is considered. Therefore, in this case, the design choice of whether the central region is transparent or opaque does not play an important role in the focusing behavior of the lens. However, when a directional transducer is employed, the enhancement factor is significantly higher than 1, which implies that the T-FZP is capable of focusing more energy in the focal area than the O-FZP, for the same number of transparent regions.

The maximum enhancement factor value is achieved when the size of the lens matches the area illuminated by the main lobe of the transducer directivity pattern. If the size of the lens is further increased, the introduction of a phase correction ring (PCR) should be considered to avoid destructive interference from the adjacent secondary lobes.[12] Although the acoustic intensity at the focus augments in both the T-FZP and O-FZP cases, the enhancement factor has surpassed its optimum value and begins to decrease. This behavior can be easily explained considering the directivity pattern of the transducer. While the Fresnel regions are illuminated by the main lobe of the directivity pattern, the inner the Fresnel region is the larger the contribution it

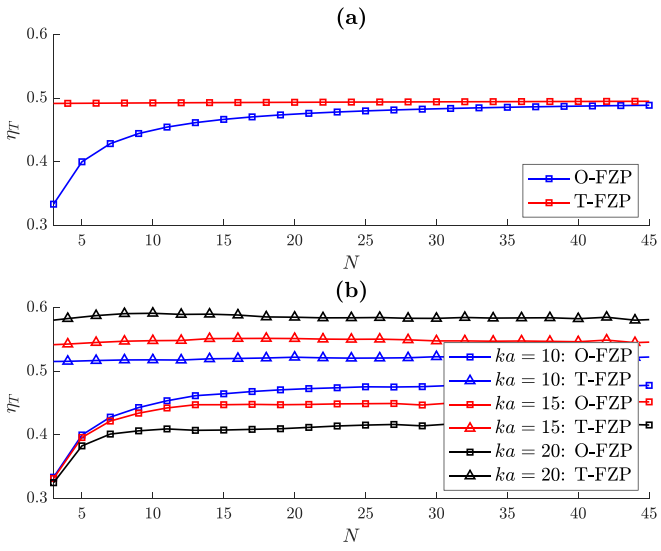

FIG. 2. Transmission efficiency: (a) plane wave incidence and (b) directional transducer placed at $d = 340$ mm from the lens.

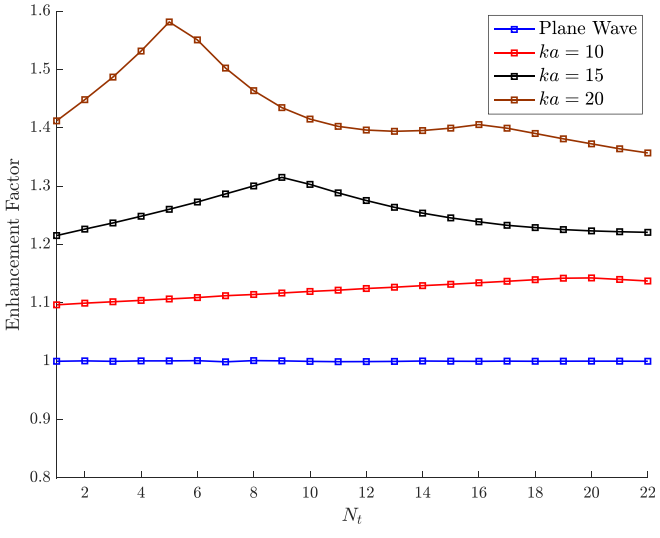

FIG. 3. Enhancement factor as a function of N_t: plane wave (blue), transducer with $ka = 10$ (red), transducer with $ka = 15$ (black), and transducer with $ka = 20$ (brown).

provides, because the main lobe presents a downward slope. However, when the secondary lobe begins to illuminate the Fresnel regions, it presents an upward slope until its relative maximum and a downward slope afterwards. Thus, the enhancement factor begins to decrease until the relative maximum of the transducer secondary lobe is reached, and after this point, the enhancement factor starts to increase again, although it does not reach the previous maximum level. This behavior is replicated when new PCRs are introduced to avoid the phase distortion effects of additional secondary lobes. Moreover, Fig. 3 depicts that when the *ka* parameter increases, the maximum enhancement factor value augments and is shifted to the left requiring a lower number of Fresnel regions. This effect is due to the fact that when *ka* increases, the transducer becomes more directional, which reduces the number of Fresnel regions that can be illuminated by its main lobe and provides a main lobe steeper slope.

Experimental measurements have been carried out in order to demonstrate the better focusing capabilities of T-FZPs over O-FZPs when directional transducers are employed. The experimental setup consists of an underwater 3D positioning system with a spatial resolution of $1 \times 1 \times 1\,\text{mm}^3$. The ultrasound signal is generated using a Panametrics Pulser and then emitted using an Imasonic piston transducer with an active diameter of 30 mm and a central frequency of 260.88 kHz. A needle hydrophone from Precision Acoustics Ltd. with a diameter of 1.5 mm is employed as the receiver. The received signal is amplified with a low noise preamplifier and then digitized using a programmable digital oscilloscope from Pico Technology.

Figures 4(a) and 4(c) show the manufactured Soret T-FZP and O-FZP, respectively. Both lenses have been designed for a focal distance of $F = 80$ mm, an operating frequency of $f_0 = 270$ kHz, and a distance between the transducer and the lens of $d = 340$ mm. One PCR has been implemented to compensate the destructive interference contributions introduced by the secondary lobes from the piston directivity pattern. The O-FZP has been manufactured with $N = 31$, while the T-FZP has been built with $N = 30$, which results in both FZPs having the same number of transparent regions, $N_t = 15$. The material selected for implementing both lenses is brass due to its high impedance contrast with water, which ensures a high reflection coefficient. Figures 4(b) and 4(d) show the measured acoustic intensity maps for the T-FZP and O-FZP cases, respectively. In these maps, *r* stands for the radial coordinate, while *z* stands for the axial coordinate. Both intensity maps have been normalized to the maximum intensity value, which is achieved in the T-FZP case. As it can be observed from Fig. 4, both manufactured lenses focus at the theoretical focal distances of $F = 80$ mm, but the T-FZP map provides a higher focal intensity value than the O-FZP map.

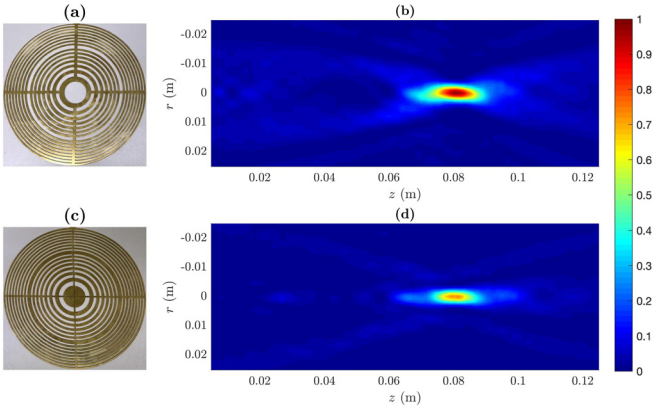

FIG. 4. Experimental results: (a) T-FZP and (b) its measured intensity map and (c) O-FZP and (d) its measured intensity map.

Figures 5(a) and 5(b) depict the measured intensity cuts along the longitudinal axis and radial axis, respectively. Simulation results are depicted with solid lines, while experimental measures are plotted with dashed lines. Although measurements and numerical results agree very well, slight differences can be appreciated at the focusing profile secondary lobes. These small differences are mainly due to the cross-shaped mechanical support of the manufactured FZPs that can be observed in Figs. 4(a) and 4(c). These structures maintain the FZP brass rings fixed in place and have not been considered in the simulation. The T-FZP lens achieves a measured intensity increase in 22.33% over the O-FZP lens at the focal distance, which results in an enhancement factor of 1.287. As it can be observed from Fig. 5(b), both measured profiles show negligible side lobes. This phenomenon is due to the piston directivity pattern, which generates a windowing effect on the incident pressure at the lens that reduces the side lobe levels in the transversal direction.

The experimental measures for the transmission efficiency of both T-FZP and O-FZP are 53.31% and 43.54%, respectively. Therefore, the enhancement on transmission efficiency is around 22.44% enhancement when using the T-FZP lens instead of the O-FZP lens. These values are in good agreement with the numerical results, which are 55.8% for the T-FZP and 44% for the O-FZP. When analyzing the focusing enhancement, results are even more significant, as the experimental enhancement factor is 1.37, resulting in a 37% enhancement when comparing intensity levels for both T-FZP and O-FZP at the focus. The numerically computed enhancement factor is 1.29, which is in good agreement with experimental measurements.

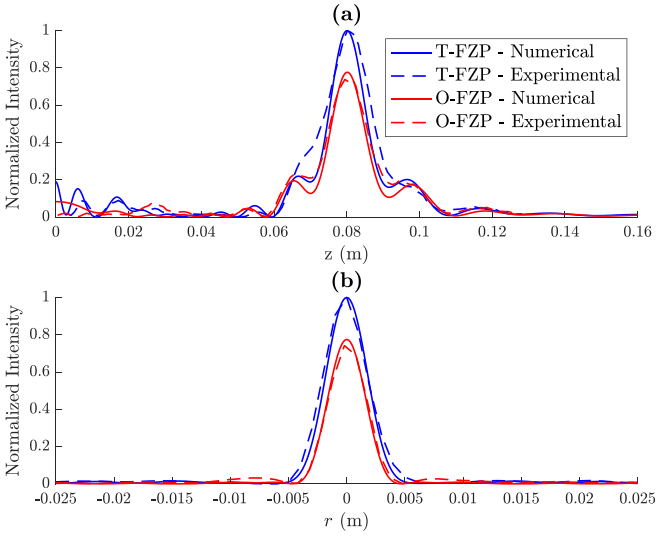

FIG. 5. (a) Longitudinal focusing profiles at $r = 0$ and (b) transversal focusing profiles at $z = F$.

In this work, a theoretical analysis of the transmission efficiency of Soret FZPs has been developed. The results show that T-FZPs and O-FZPs offer almost identical focusing performance for plane wave incidence. Thus, the decision of whether the central region is transparent or opaque in this case is marginal. However, when a directional transducer is employed as the emitter, which is the common case in most underwater ultrasound applications, T-FZPs provide higher focusing intensity levels than their corresponding O-FZPs. Moreover, as the transducer becomes more directional, the transmission efficiency gap between T-FZP and O-FZP cases increases. Experimental measurements have been carried out, showing good agreement with theoretical simulations. The manufactured T-FZP achieves an enhancement factor of 1.37. Therefore, this work demonstrates that the a T-FZP is a better design option than an O-FZP for underwater focusing applications employing directional transducers.

This work was supported by Spanish MINECO TEC2015-70939-R and MICINN RTI2018-100792-B-I00 projects. S.P.-L. acknowledges financial support from Universitat Politècnica de València Grant Program No. PAID-01-18.

REFERENCES

[1]J. Chen, J. Xiao, D. Lisevych, A. Shakouri, and Z. Fan, Nat. Commun. **9**, 4920 (2018).
[2]Z. Liang and J. Li, Phys. Rev. Lett. **108**, 114301 (2012).
[3]Y. Li, B. Liang, X. Tao, X. F. Zhu, X. Y. Zou, and J. C. Cheng, Appl. Phys. Lett. **101**, 233508 (2012).
[4]Y. Li, G. Yu, B. Liang, X. Zou, G. Li, S. Cheng, and J. Cheng, Sci. Rep. **4**, 6830 (2015).
[5]J. P. Xia, X. T. Zhang, H. X. Sun, S. Q. Yuan, J. Qian, and Y. Ge, Phys. Rev. Appl. **10**, 014016 (2018).
[6]L. Kipp, M. Skibowski, R. L. Johnson, R. Berndt, R. Adelung, S. Harm, and R. Seemann, Nature **414**, 184 (2001).
[7]R. S. Rodrigues Ribeiro, P. Dahal, A. Guerreiro, P. A. Jorge, and J. Viegas, Sci. Rep. **7**, 4485 (2017).
[8]H. D. Hristov and M. H. Herben, IEEE Trans. Microwave Theory Tech. **43**, 2779 (1995).
[9]H. D. Hristov and J. M. Rodriguez, IEEE Microwave Wireless Compon. Lett. **22**, 574 (2012).
[10]M. Molerón, M. Serra-Garcia, and C. Daraio, Appl. Phys. Lett. **105**, 114109 (2014).
[11]D. C. Calvo, A. L. Thangawng, M. Nicholas, and C. N. Layman, Appl. Phys. Lett. **107**, 014103 (2015).
[12]S. Pérez-López, J. M. Fuster, P. Candelas, C. Rubio, and F. Belmar, Appl. Phys. Lett. **112**, 264102 (2018).